Magnetic properties of two copper (II) halide layered perovskites
by Nava Rabiner Sivron

A thesis submitted in partial fulfillment of the requirements for the degree of Master of Science in Physics
Montana State University

Abstract:
The magnetic moments of Copper(II) halide perovskite salts (3AP)CuX4, where X stands for Br or Cl, have been reported for the first time.

The experimental results are explained by the Baker model, which is a high T expansion of the Heisenberg Hamiltonian for a square lattice combined with a molecular exchange field correction.

Both compounds demonstrate an antiferromagnetic exchange between the layers, since the value measured for the exchange parameter is negative. J2h = -57±7 for (SAP)CuBr4 and -25±1 for (SAP)CuCl4. Both salts demonstrate ferromagnetic exchange within the layer, with positive Jlh = 15±1 for the Cl compound and 20.512.5 for the Br.

The interaction is stronger for (SAP)CuBr4 than for (SAP)CuCI4 as the absolute values of both Jlh/k and J2hZk are larger for the bromide compound. The antiferromagnetic exchange is dominant for both samples. For the bromide salt this result is more evident, as the ratio J2hZJih is larger.

The Cu-X and the X-X bond lengths are found to affect the strength of the exchange interaction in a similar way to other salts. Longer bonds result in weaker interaction. The natural logarithm of X-X bond length and the natural logarithm of J2hZk obey the linearity which was previously found for (nDA)CuX4 series of compounds.

MAGNETIC PROPERTIES OF TWO COPPER (II) HALIDE LAYERED PEROVSKITES

by

Nava Rabiner Sivron

A thesis submitted in partial fulfillment
of the requirements for the degree

of

Master of Science

in

Physics

MONTANA STATE UNIVERSITY
Bozeman, Montana

August 1992

APPROVAL

of a thesis submitted by

Nava Rabiner Sivron

This thesis has been read by each member of the thesis committee and has been found to be satisfactory regarding content, English usage, format, citations, bibliographic style, and consistency, and is ready for submission to the College of Graduate Studies.

8/21/92
Date

Chairperson, Graduate Committee

Approved for the Major Department

8-24-92
Date

Head, Major Department

Approved for the College of Graduate Studies

8/31/92
Date

Graduate Dean

STATEMENT OF PERMISSION TO USE

In presenting this thesis (paper) in partial fulfillment of the requirements for a master's degree at Montana State University, I agree that the Library shall make it available to borrowers under the rules of the Library.

If I have indicated my intention to copyright this thesis (paper) by including a copyright notice page, copying is allowable only for scholarly purposes, consistent with "fair use" as prescribed in the U.S. Copyright law. Requests for permission for extended quotation from or reproduction of this thesis (paper) in whole or in parts may be granted only by the copyright holder.

Signature _____

Date Aug 25 1992

ACKNOWLEDGEMENTS

First of all, I would like to thank my advisor, Prof. John E. Drumheller, for his patience, time and the helpful advice he gave me. Many thanks to Todd Grigereit for all the help he gave me, and to all my colleagues: K.Ravindran, Bob Parker, Liu Ying and Dan Teske. I would also like to thank Dr. Ken Emerson from the Chemistry Department of M.S.U. for all he taught me. Many thanks to Norm Williams - the machine shop supervisor, and to Eric Anderson, and to Ran Sivron, my husband, for all his comments, help and love. Without those wonderful people this work would never have been completed.

TABLE OF CONTENTS

LIST OF TABLES

LIST OF FIGURES

LIST OF FIGURES-Cont'd

ABSTRACT

The magnetic moments of copper(II) halide perovskite salts $(3AP)CuX_4$, where X stands for Br or Cl, have been reported for the first time.

The experimental results are explained by the Baker model, which is a high T expansion of the Heisenberg Hamiltonian for a square lattice combined with a molecular exchange field correction.

Both compounds demonstrate an antiferromagnetic exchange between the layers, since the value measured for the exchange parameter is negative. J_{2h} = -57±7 for $(3AP)CuBr_4$ and -25±1 for $(3AP)CuCl_4$. Both salts demonstrate ferromagnetic exchange within the layer, with positive J_{1h} = 15±1 for the Cl compound and 20.5±2.5 for the Br.

The interaction is stronger for $(3AP)CuBr_4$ than for $(3AP)CuCl_4$ as the absolute values of both J_{1h}/k and J_{2h}/k are larger for the bromide compound. The antiferromagnetic exchange is dominant for both samples. For the bromide salt this result is more evident, as the ratio J_{2h}/J_{1h} is larger.

The Cu···X and the X···X bond lengths are found to affect the strength of the exchange interaction in a similar way to other salts. Longer bonds result in weaker interaction. The natural logarithm of X···X bond length and the natural logarithm of J_{2h}/k obey the linearity which was previously found for $(nDA)CuX_4$ series of compounds.

CHAPTER 1

INTRODUCTION

In 1988 the crystal structures of two new copper (II) halide layer perovskite salts were reported for the first time. The special interest in the 3-ammoniumpyridinium tetrabromocuprate(II) and 3-ammoniumpyridinium tetrachlorocuprate(II), arose from the fact that they were non centrosymmetric. Predictions about their magnetization, made by comparison with other crystals were limited, and subject to the fact that insufficient data had existed to make satisfying correlations for the tetrahedrally distorted anions.[1] It was expected that the strength of the exchange interaction for the bromide salts would be greater than for the chloride salts. The samples were expected to demonstrate a ferromagnetic exchange inside the layer and antiferromagnetic exchange between the layers.

In this work the crystal growth was repeated according to the literature, and the powder susceptibility was measured, both by cooling and by heating. The data was interpreted using the Baker model Heisenberg high temperature series expansion for a square lattice, combined with a molecular exchange field correction.[7,10]

A detailed explanation of the structure of the crystals and how it relates to the predictions of the magnetic behavior of the samples is given in chapter 2, as well as

information pertaining to the crystal growth. Estimates of the accuracy and signal stability of the Vibrating Sample Magnetometer which was used to measure the magnetization are given in chapter 3. The new results for the powder susceptibility as well as comparison with other compounds are presented in chapter 4, and discussed in chapter 5 - the conclusion. The current chapter gives the reader the necessary theoretical background needed to understand the models used.

Theoretical Background

The macroscopic magnetic behavior of the magnetic moment M depends on the field H and susceptibility χ of the material:

$$M=\chi H \qquad (1)$$

The most general equations used to describe the susceptibility are given by the Curie law, $\chi = C / T$, and Curie-Weiss law, $\chi = C /(T-\theta)$,[1,2,3] where C is the Curie constant, T is the temperature and θ is a positive constant for ferromagnets, and negative for antiferromagnets.

According to the simplest models, the absolute value of θ is almost equal to the critical temperature Tc, at which long range order is obtained. This, however, is not always true. For example, short range order can cause the ratio Tc/θ to be different than one. In some models only short range order exists at temperatures above zero. For

example, the calculation for a linear Heisenberg chain for spin 1/2 yields[2,6] the result that the 1D systems do not have a non zero Tc.

The Curie law and the Curie Weiss law for spin 1/2 systems are shown[2] to be the result of an exact calculation which assumes long range order only, and uses the partition function to calculate the magnetization. The microscopic magnetization μ, which is the mean z component of the magnetization of an atom is determined[2] from the well known statistical mechanics results

$$\overline{\mu}_z = kT\frac{\partial \ln Z}{\partial H} \tag{2}$$

$$Z = \text{trace}\left\{ e^{\mathcal{H}/kT} \right\} = \sum_i e^{\varepsilon_i/kT},$$

where k is the Boltzman constant, Z is the partition function,[3,8] $\mathcal{H}$ is the Hamiltonian and ε_i are the energy levels accessible to the atom.

If M_z is the average macroscopic magnetization per mole in the z direction, then

$$\overline{M}_z = N_0\overline{\mu}_z, \tag{3}$$

where N_0 is avogadro's number. From equations (1), (2) and (3) we get

$$\chi = \frac{N_0 kT}{H}\frac{\partial \ln Z}{\partial H} \tag{4}$$

The difference between the Curie law and the Curie Weiss law comes from the difference in the Hamiltonians used. For the Curie law, only the Zeeman term is taken

into account, and the following Hamiltonian is used

$$\mathcal{H} = - g \mu_B S_{jz} H_z, \quad (5)$$

where μ_B is the Bohr magneton, S is the spin of the electron of the j atom and g is the Lande factor.

For the calculation of the Curie Weiss law an additional term is used in the Hamiltonian, based on the assumption that a perturbation in the form of an additional internal field H' is added to the external field. This perturbation can be caused by the presence of an exchange interaction.[3] The additional term in the Hamiltonian is written as

$$-g\mu S_{jz}H' = -2JS_{jz}\sum_{k=1}^{n} S_{kz}, \quad (6)$$

where n is the number of nearest interacting neighbors of the atom, J is the exchange parameter and H' is the molecular exchange field.

By using the new Hamiltonian, the following result is obtained[3]

$$\chi = \frac{N_0 g^2 \mu^2 j(j+1)}{3k(T-\theta)} = \frac{C}{(T-\theta)}, \quad (7)$$

where j is the sum of the quantum number of the spin and the orbital angular momentum of the atom.

The exchange interaction isn't always direct. There are compounds in which it occurs through a bridging ion.[2] The absolute value of the exchange parameter J, depends on the overlap of the electron orbitals. When the value of J is positive, the spins tend to

align parallel to one another and the sample has a ferromagnetic exchange. When the value of J is negative the spins favor an anti-parallel configuration.[1]

The exchange interaction is used in many models. In our case it is represented by the Heisenberg Hamiltonian

$$\mathcal{H}=-2J\Sigma_{ij} (S_{ix} S_{jx}+S_{iy} S_{jy}+S_{iz} S_{jz}). \quad (8)$$

This Hamiltonian is used when there is no preferred direction present, and thus the local spin operators don't commute with the Hamiltonian.[4] The Heisenberg model does not assume any restriction on the spin orientations. Copper, which is used in this work, offers a good example of a Heisenberg system.[2]

The sources for the magnetic moment demonstrated by the sample are the following[1]:

1. Spin
2. Orbital angular momentum about the nucleus
3. A change in the orbital moment induced by an applied field.

In our case, the first is the most important, since the third has been shown to be independent of temperature and field. According to Lenz's law it will result in a diamagnetic effect and yield a negative susceptibility. The second is assumed to be negligible in spite of the fact that the orbital magnetic moment of copper is not zero, for the following reasons:

The Copper (II) ion has nine d electrons outside the argon core. It has s=1/2

configuration, no matter what geometry the ion is placed in.[2] The $[Ar](3d)^9$ configuration has j=5/2 and l=2. Therefore spin orbit coupling should be important in Cu(II) ions. When the 3d shell is more than half full [1] the g values should be greater than two.[2]

Since the effective Bohr magneton depends on the g value, theory predicts that it would be large. But when the prediction is checked, a surprising result comes out[28]: the effective Bohr magneton for the iron transition group is found to be in poor agreement with the experimental results. For this group, the correct value is obtained by assuming that the orbital momentum is "quenched".[2]

Using this assumption, in our case for copper compounds, the atomic magnetic moment, which is written as $\mu_{eff} = g\,[j(j+1)]^{1/2}\,\mu_B$ with

$$g_j = 1 + \frac{s(s+1) - l(l+1) + j(j+1)}{2j(j+1)}$$

yields

$$\mu_{eff} = g_j\,[s(s+1)]^{\frac{1}{2}}\,\mu_B. \qquad (9)$$

Because of the fact that the orbital contribution is largely quenched[2] and there is no zero field effect for spin 1/2, the g value is not large for copper. An example is given by $g^{\parallel}=2.38$ and $g^{\perp}=2.06$ for the sample $K_2CuCl_4 \cdot 2H_2O$.[2]

In our experiment the powder magnetic susceptibility is measured, thus the measurements refer to the value of the average susceptibility $\langle\chi\rangle$ only, obtained from[2]:

$$\langle\chi\rangle = (\chi^{\parallel}+2\chi^{\perp})/3, \tag{10}$$

or

$$\langle\chi\rangle = 1/3\ (\chi_x+\chi_y+\chi_z). \tag{11}$$

Since the g value is averaged too, it should be in the range[2] $2 < g < 2.3$.

To calculate the specific behavior of our crystals, more sophisticated models should be used. The models need to include information pertaining to the ion interaction with the crystal as well as to take into account that further complication that arises from the fact that the intralayer magnetic behavior may or may not be of the same nature of that of the layer.

In our case, the crystal structure is made of two dimensional layers stacked in an eclipsed conformation. A two-dimensional model is used for the determination of the intralayer value of the exchange interaction parameter J_{1h}, whose value should reveal whether the intralayer behavior is ferromagnetic or antiferromagnetic in its nature. The Baker model[7] used to calculate the exchange interaction parameter of the layers, is a high temperature susceptibility series expansion obtained for the spin 1/2 Heisenberg model for a square lattice. In their work Baker, et al.[7] add more coefficients to the ones previously obtained by Rushbrooke, et al.[8] Their calculations use the Hamiltonians in equations (5) and (8). From these Hamiltonians they calculate the partition function (see equation (2)) and expand it in powers of J_{1h}/kT. Finally the susceptibility is calculated by

$$\chi = \frac{\partial^2 (N_0 kT \ln Z)}{\partial H^2}. \tag{12}$$

This relation is equivalent to equation (4).[3]

Using the final result of their work:

$$\chi T = C\left(1+\sum_{n\geq 1}^{10} \frac{a_n}{2^n n!} x^n\right), \qquad (13)$$

where

$$C = \frac{N_0 \mu_{eff}^2}{3k} = N_0 g^2 \mu_B^2 \frac{S(S+1)}{3k}$$

and

$$x = \frac{J_{1h}}{kT}$$

and a_n are:

a_1=4 a_2=16 a_3=64 a_4=416 a_5=4544

a_6=23488 a_7= (-)207616 a_8=4205056 a_9=198295552 a_{10}= (-)2574439424

This formula is used to find the value of the intralayer exchange parameter. However the effect of the interlayer parameter J_{2h} is still needed to be taken into account. As previously mentioned the exchange interaction can be added in the form of a correction to the external magnetic field, as shown in previous work[10,11]

$$M_i = \chi_i (H_i + H'_i) . \qquad (14)$$

By using the molecular exchange field expression[2,10] the susceptibility is

calculated

$$H'_i = \frac{2ZJ}{N_0 g_i^2 \mu_B^2} \chi'_i H_i, \qquad (15)$$

where H'_i is the molecular exchange field, Hi is the external field, χ_i is the zero perturbation order susceptibility and χ'_i is the exchange corrected susceptibility actually measured. From equations (14) and (15)

$$\chi'_i = \lim_{H_i \to 0} \frac{M_i}{H_i} = \frac{\chi_i}{1 - (2ZJ_{2h}/g_i^2 \mu_B^2)\chi_i}. \qquad (16)$$

Thus by using the experimental results for χ'_i once again and the previous zero order calculation for χ_i, the interlayer exchange parameter J_{2h} is obtained.

CHAPTER 2

SAMPLE STRUCTURE AND PREPARATION

The magnetic behavior of the perskovite salts samples cannot be well understood without looking at their structures. At the beginning of this chapter the crystal growth technique is described. The second part of the chapter contains information pertaining to the structure of the samples and it's correlation to the values of the exchange parameters.

Sample Preparation

The crystals were prepared by evaporation of concentrated HX solution that contained CuX_2:(3AP) with ratio somewhat greater than one, where X stands for either Cl or Br.[1] In order to avoid competing reactions and the formation of the compound $(3AP)_2Cu_2X_6$ the strength of the acid solutions was required to be greater than 1M.[1,2]

To grow the samples we performed the following steps:

1. HX in H_2O solution was slowly added to (3AP), allowing the reaction heat from

$$H_2O + (3AP)^{2+} HX \rightarrow [(3AP)^{2+} H_2] X_2 + H_2O$$

to escape.

2. H_2O was added drop by drop to the CuX_2, until a uniform solution was formed. (No more H_2O was used than the minimum required in order to dissolve the CuX_2.)

$$H_2O + [\,(3AP)\,H_2^{2+}X_2\,] \rightarrow (3AP)\,CuX_4 + H_2O$$

After the solutions were mixed together, the crystals formed slowly by evaporation, and when ready they were washed with EtOh, and left to dry.

The following ratios were used to calculate the appropriate amounts needed for the above process:

(3AP)	:	HX	:	CuX_2
1	:	2	:	1.2

Because of the requirement for high acidity we used a concentration of approximately 6M HCl in H_2O, and approximately 7M HBr in H_2O. After two days of slow evaporation the crystals formed as green flat plates for the chloride salts, and dark opaque plates for the bromide salts.

In order to avoid large background signals the sample holder was prepared from teflon, which has a very small magnetic permeability. It was treated in the following ways:

1. Washed with soap, distilled water, 50% methanol and 50% acetone mixture.
2. Pickled ultrasonically with 10% nitric acid solution inside an ultrasonic device.

Crystal Structure

The salts consist of two dimensional perovskite type $(CuX_4)_n$ layers, interleaved by the organic cations $(3AP)^{2+}$.[1] The 3-aminopyridine cations bridge between layers with the ammonium group NH_3 and the pyridinium NH^+ group hydrogen bonding to adjacent layers. The NH^+ group forms N-H···X hydrogen bonds with CuX_4^{2-}. The three hydrogen atoms of the ammonium group (NH_3) each form a hydrogen bond, one to a bridging halide ion and two to non bridging halide ions.[1]

To understand the interlayer structure and how it relates to the magnetic behavior of the samples we need to use the following information: The ability of the Cu···X distance to vary over a large range makes it possible to change the size of the cation used, and to vary the magnetic properties systematically. The (3AP) cation is used in our work. Considering the stacking of the layers it is found[1] that the relatively small size of the 3-aminopyridine plays an important role in term of the stacking of adjacent layers. It leads to short interlayer halogen-halogen distances. Thus short X···X contacts are created between the layers which are referred to as interlayer distances — 3.992Å for X=Cl and 3.889Å for X=Br.

The value of J_{2h}, the interlayer exchange parameter depends on the X···X bond length (2h stands for the two halides in the linkage Cu-X···X-Cu between the layers). J_{2h} is expected to decrease when the bond length increases, since the differential overlap between the two magnetic ions depends on it. This trend is experimentally demonstrated for a series similar to the one we use — the $nDACuX_4$ series, in which n varies from 2

to 5.[1]

The layers are found to be stacked in an eclipsed conformation, as seen in Figure 1 in which the linkage between layers was demonstrated.

From the crystal structure it is concluded[1] that J_{2h} depends on:

1. X···X, the contact distance between layers. J_{2h} gets bigger when X···X gets smaller.)
2. The angle Cu-X···X. J_{2h} gets bigger when this angle is closer to 180^0.
3. The Cu-X distance of the interlayer linkage Cu-X···X-Cu. J_{2h} gets bigger when the Cu—X distance gets smaller.

The next step is to try and understand the intralayer structure, and how it relates to the magnetic behavior of the sample. Once again, we need to use the information given in reference [1]. It is found that the layers consist of $(CuX_4^{2-})_n$ arrays. The arrays are found to be approximately two dimensional, since although the anions are found to be tetrahedrally distorted the bridging angle Cu-X···Cu is only 161.2^0 for chloride and 157.6^0 for bromide. The two dimensional structure is non centrosymetric, as seen in Figure 2 and Figure 3. The chloride Cu-X distance is 2.28Å, and the semicoordinate bond Cu···X is of the order of 3.25Å. The bromide Cu-X distance is found to be 2.428Å and the Cu···X distance is of the order of 3.35Å.

Since the absolute value of J_{1h} depends on the extent of the differential overlap between the two magnetic orbitals, it is assumed[1] that there should be a strong

dependence on the Cu···X bond length. J_{lh} is expected to decrease when the bond length increases, although variations in the coordinate Cu-X influence the J_{lh} absolute value as well. The differential overlap depends on the Cu···X bond for another reason: it affects the tetragonality of the (CuX_4^{2-}) groups.

Experimental results for J_{lh} for compounds containing bromine reveals that its value is 50% - 100% larger than for those containing chlorine.[1] Bromine, being more polarizable than chlorine, frequently allows larger superexchange interaction. However bromine is also a larger ion, and hence separates the metal ions further apart.[3]

A summary and additional data pertaining to these compounds (obtained from the literature) is listed in Table 1.

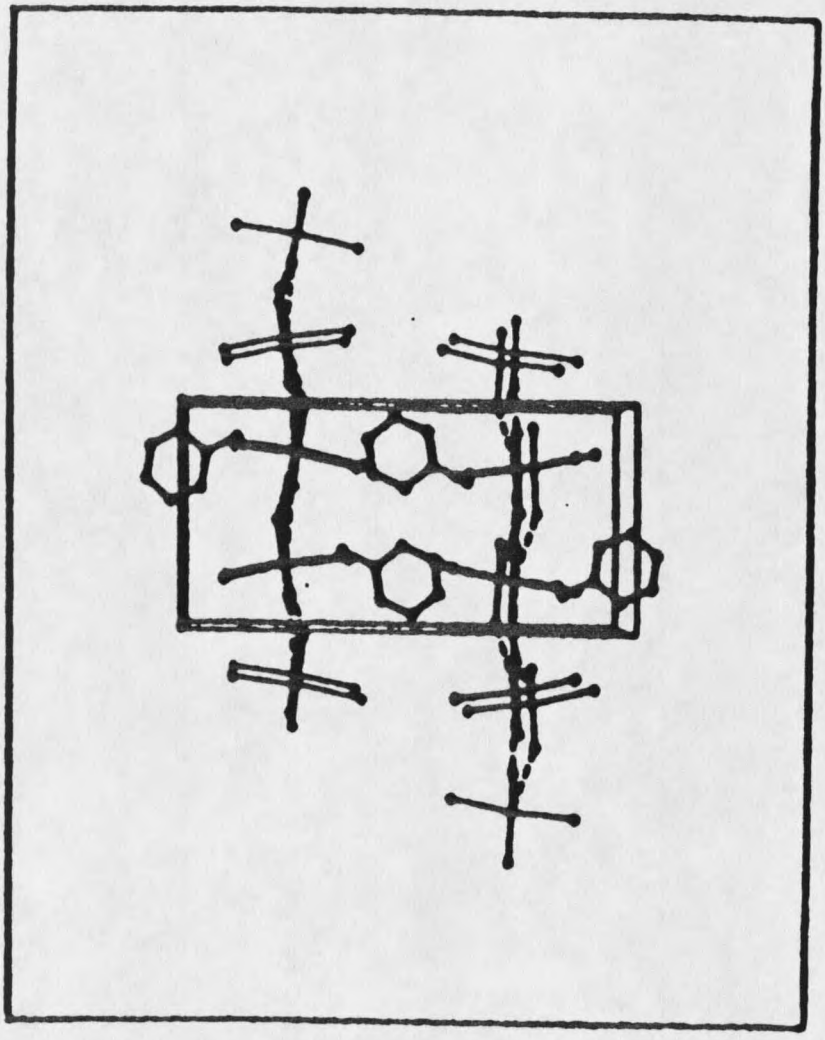

Figure 1 A side look at the layers reveals the eclipsed structure and shows how the layers are linked. The c axis of the monoclinic crystal is horizontal and the b axis is vertical.

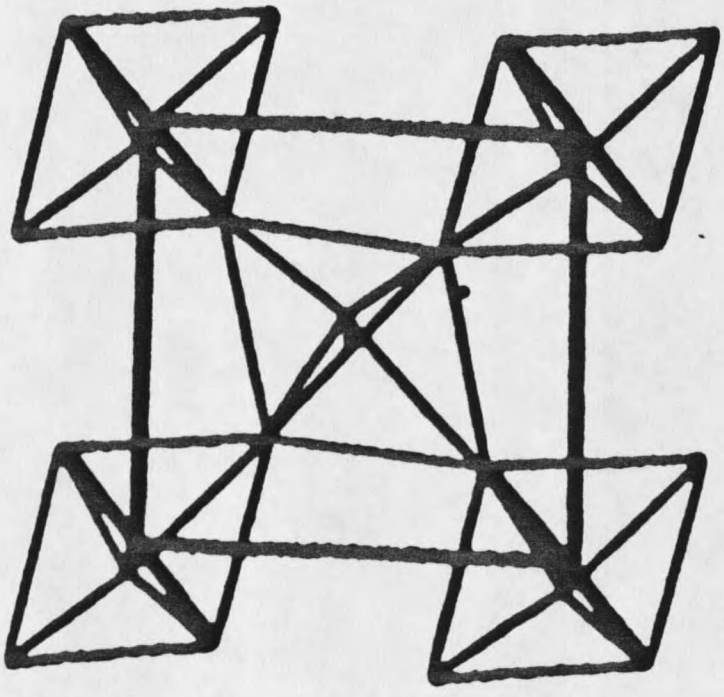

Figure 2 A look at the two dimensional noncentrosymmetric structure of the layer.[1]

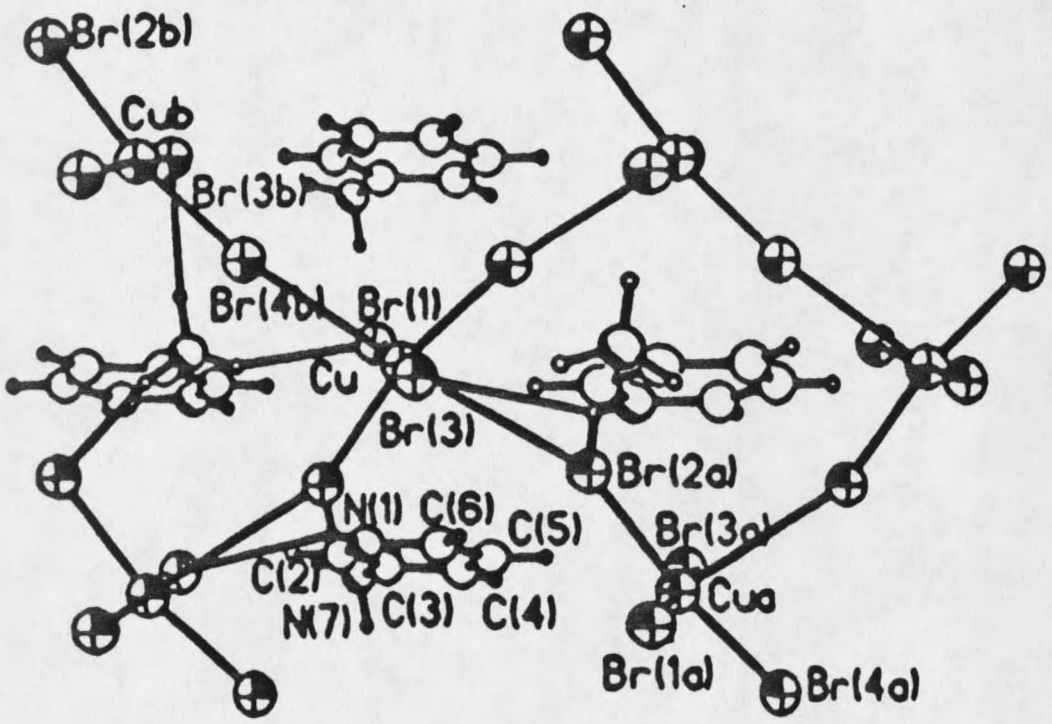

Figure 3 A look at the atomic structure of the layer.[1] The b axis of the monoclinic crystal is horizontal and the a axis is vertical. Each Cu atom has 4 Cu neighbors inside the layer, bridged by one X halide, and 2 Cu neighbors from adjacent layers, bridged by 2 X halides.

Table 1 Structural information of (3AP)$CuBr_4$ and (3AP)$CuCl_4$.

	(3AP)CuX_4 compounds:	
	X=chloride	X=bromide
Crystal parameters:		
Cu—X···X bridging angle (in the layer)	161.2	157.6
X—Cu—X trans angle (out of the layer)	170.56	170.6
Cu—X···X angle	163.5	165.3
X···X distance	3.992Å	3.899Å
bond distance Cu—X	2.28Å	2.428Å
semicoordinate bond distance Cu···X	3.183;3.339Å	3.266;3.478Å
monoclinic crystal parameters a:b (layer parameters) c:	 6.941;8.384Å 16.848Å	 7.179;8.766Å 17.218Å
monoclinic crystal angle	94.63	95.29
$g^{\parallel}$	2.160	Unknown
$g^{\perp}$	2.052	Unknown

CHAPTER 3

EXPERIMENTAL INFORMATION

In any experiment the stability, repeatability and calibration of the system are crucialbecause they determine the accuracy of the measurements. Possible sources for errors as well as the steps taken to minimize them are described in this chapter.

To measure the powder susceptibility of the samples a Vibrating Sample Magnetometer (V.S.M) model 155 was used. The following preliminary operational steps were taken:

1. Electronic checks, noise checks and overload checks were performed according to the instructions of the operating and service manual. The performance was good.
2. The signal stability was checked and the system accuracy was estimated by looking at the data that was obtained at constant temperature over time periods of the order of those required for a normal measurement (the results are discussed later in the chapter).

3. Efficiency checks were made by looking at the helium consumption and the time needed to complete measurements of the full temperature range. Helium consumption estimates for various flow rates were tabulated during each experiment. The table of flow rates and temperature variations which was made according to the data was used to find out how to get maximum results from the system at minimum time and helium consumption. Thus a way to operate the system efficiently was found and will be discussed later in this chapter.
4. Calibration was made by using nickel and $HgCoSCN_4$ samples. See results at the end of this chapter.

General estimates of the system stability at the VSM interface magnetic moment scales 0.01, 0.1 and 1 for large and small signals at both ends of the temperature range gave the following results:

An empty system would give fluctuations of the order of ± 0.00004 emu*Oe at room temperature. This is the minimal error expected from the system. Since most of the samples have a small signal at room temperature, the percent error rises when measurements are made at that temperature. The $(3AP)CuX_4$ samples, for example, have signals of the order of 0.002 at room temperature. These fluctuations would result in large errors of magnitude ± 2%.

The percent error due to background fluctuations is ± 3% for the teflon sample holder at 294K. The order of magnitude of the fluctuations in teflon background is 0.0006

emu*Oe at room temperature, which is 30% of the fluctuating signal. These results indicate that the room temperature measurements would be extremely difficult to interpret. The signal for teflon at low temperature is larger, of the order of 0.01, and so the percent error reduces to ± 0.8%. That, and the fact that this signal is 1% of the $3APCuX_4$ signal make it possible to obtain better results for the low temperature range.

For the nickel sample, which is used for the calibration and is measured on the 1 scale, the fluctuations are ± 0.1% emu*Oe at room temperature. Another reason for inaccuracy in the calibration with nickel is the fact we only calibrate with an accuracy of ± 0.01 emu*Oe. This inaccuracy should be negligible for large signals, but may not be negligible for extremely small signals. The day to day repeatability was checked as well during the calibration and showed variations of ± 0.35% for nickel.

Other parameters which can influence the accuracy of the measurements are:

1. The instability in the flow rate of helium can cause fluctuations in the temperature. At 4.2 K, where the flow should be the steadiest, because the needle valve which leads helium to the sample is open wide, the magnetic moment of nickel has shown fluctuations of the order of 0.04 emu*Oe corresponding to 0.5% error. At the 10-20K range the stabilizing of the system at a single temperature over a long period of time is extremely difficult, resulting in an inaccuracy of ± 1% in the signal for a 0.01 scale.
2. If the sample is placed inside the teflon sample holder the magnetic field will be

reduced by 0.2% because of shielding. The magnetic field demonstrated instability of the order of 5 oe. The accuracy of the magnetic field probe was checked by measuring the field of a well known permanent magnet, and was found to be ±0.01%.

3. The relative position between the sample and the pickup coils: The size of the detecting coils limits the size of the sample that these coils can detect with a constant response. For the nickel sphere the signal was at a constant peak for a motion of 0.1 cm up or down with respect to the pick up coils. If the motion continues the signal changed by 0.2%. It remains constant for additional 2.5 cm relocation in each direction. Therefore 0.5 cm is the maximal recommended size for the sample, yielding a 0.2% error. The XYZ alignment which positions the sample with respect to the pick up coils is extremely important. Its repeatability must be checked, since it has its own mechanical limitations. Upon taking the nickel sample out and inserting it back in a ± 0.4% change in the signal was observed.

   The response of the rod which holds the sample to cooling and heating could lead to small differences in the geometry and change the signal picked by the pickup coils.

4. The temperature detector and the sample are not located at exactly the same place, and the response of the sample to the flow changes may be different from the response of the detector,depending on the heat capacity of both. This can cause

hysterasis: The cooling curves look different than the heating curves. For example, if the response of the detector is faster than the response of the sample, the temperature readings of the heating curve will be too high, thus shifting the whole curve towards higher temperatures, and that of the cooling curve too low, thus shifting the curve towards lower temperatures. However, the situation may not be so simple, as the heat capacity varies with different temperatures, especially at the phase transition range. For the (3AP)$CuBr_4$ sample, variations between cooling and heating as large as 8% are observed theoretical reasons as well. To minimize this effect cooling as well as heating measurements were done. Since heating and cooling play an important role in the measurements these results were interpreted separately and compared.

The response of the system to cooling and heating as a function of the helium flow rates was made. The interested reader will find the necessary information needed to the V.S.M user to plan and estimate the time and helium consumption needed for the measurements. For a given flow, the rate of change of temperature with time, $\partial T/\partial t$ varies with the temperature. This affects the helium consumption needed to complete the measurement at that range. A higher flow consumes more helium, but also covers the temperature range faster so that overall the efficiency may be better. The efficiency is represented by $(\partial He/\partial T)$, the helium consumed to cover temperature interval of 1K.

The user must also consider that flow rates that are too high result in large

temperature variations, which may be too fast for a particular sample. The signal stability must be obtained to achieve good data. Each sample has its own response and the appropriate method should be determined individually. However the system response can be well predicted by use of the Tables 2, 3.

Table 2 Helium consumption in %, and temperature variation in degrees Kelvin /min as a function of helium flow rates in cc/min. The flow numbers could change if the V.S.M. top is sealed in a different way than it did when this table was made. This table is for cooling.

	20-40K		40-70K		70-100K		100-200K		200-300K	
	∂T/∂t	∂He/∂t	∂T/∂t	∂He/∂t	∂T/∂t	∂He/∂t	∂T/∂t	∂He/∂t	∂T/∂t	∂He/∂t
Flow Rates cc/min										
200	No cooling		No cooling		No Cooling		No cooling		2.4	0.2%
300	"		"		"		2.5	0.1%		
400	"		"		3	0.07%	6.0	0.03%		
500	"		1.3	3.5%	4	0.05%	9.0		8.0	1.0%
600	"		4.5	0.15%	5.5	0%				
700	6	0%	7	0%						
800	6.5	0.6%	8	0.2%						
900	7	0.2%	10	0.5%	9	0.5%				
1000	7.5	0.1%								

∂T/∂t is measured in Kelvin per minute
∂He/∂T is measured in percent per Kelvin

Table 3 Helium consumption in %, and temperature variation in degrees Kelvin /min as a function of helium flow rates in cc/min. The flow numbers could change if the V.S.M. top is sealed in a different way than it did when this table was made. This table is for heating.

	20-40K		40-70K		70-110K		110-170K		170-250K	250-300K
	∂T/∂t	∂He/∂t	∂T/∂t	∂He/∂t	∂T/∂t	∂He/∂t	∂T/∂t	∂He/∂t		
								He(cc/min)		
Flow Rates cc/min										
0			4		2		1-0.5	0.4%	No heating	
100			3		1.5	0.1%	No heating		"	
200			2		No heating		"		"	
300			1		"		"		"	
400	10	0.2%	1		"		"		"	
500	8		0.5		"		"		"	
600		0.6%	No heating		"		"		"	
700	No heating		"		"		"		"	
800	No heating		"		"		"		"	
900	"		"		"		"		"	
1000	"		"		"		"		"	

The following procedure allows the V.S.M user to obtain four files with one helium transfer only. These files can be used to determine the sample response to heating and cooling. By comparing the difference between the files the user can estimate how slowly the measurements should be done.

1. A cooling file which covers the full temperature range is obtained by cooling slowly at:

   200 cc/min for the range 300-200K

   then 350 cc/min for the range 200-80K,

   then 450cc/min for the range 80-40K,

   and finally the flow is gradually changed by hand to cover the 20-4.2K range. This took 1 3/4 hour and consumed 50% of the helium.

2. A heating file for the range 4.2-130K is obtained by:

   A gradual change of the flow rate to cover the 4-40K range

   then 300 cc/min to cover the 40-60K range

   then 100cc/min to cover the 60-130K range.

3. A cooling file which is done quickly, and gives some information about how fast the sample can respond to changes in temperature (by comparing to the slow cooling curve obtained at the first step).

   600 cc/min for the range 130-20K.

   The flow is changed as necessary to cover the 20-4 K range. The previous two steps consume 42% of the helium, and only 8% helium is left. They take 1/2 an hour.

4. A heating file which is done at the rate necessary to cover the range 4-40, by gradual change of the flow.

   Then 150 cc/min is used to cover the 40-70 range, which consumed all of the helium that is left. Once the helium is finished, the system slowly heats up to cover the full temperature range left. This step takes 2 1/2 hours. Careful attention should be taken not to use up all the helium before the 70K temperature is obtained. If, for example, the helium level drops to zero before that the system temperature can instantaneously skip from 20K to 70K.

To calibrate the system, a pure nickel sphere sample was used. The one point calibration value required for the calibration knob was determined at room temperature according to the formula:[2]

$M=w*54.95[1-12/H][1-0.0003(298-T)]$;

where w is the mass of the sample in gm, H is the magnetic field in Oe and T is the temperature, which is the room temperature and is close to 298K. M is the magnetization in emu*Oe.

Since the theoretical value accuracy is 0.4%[2], a signal of 3.51 emu*Oe would have an error of ±0.014 emu*Oe.

The system was then checked at 4.2K, for which the magnetic moment for nickel was calculated according to the value[2]

$M=58.19*w=3.7357$ emu*Oe.

Since the system gave a value that was different by 0.1 emu *Oe from the

expected value, the calibration was repeated this time at low temperature, and the value at room temperature was checked again. At room temperature, the magnetization value showed an error of the order of 0.1 emu*Oe. Repeating the calibration a few times at low and high temperatures confirmed that a 2.8% discrepancy was present over the full temperature range. Therefore the full range was checked by another sample.

The full temperature range was measured for the sample ($HgCo(NCS)_4$)-whose magnetic behavior is well known.[1] The inverse susceptibility vs. temperature plot for this sample should give a linear relation as shown in figure 4. This linear relation was indeed obtained by the Vibrating Sample Magnetometer at the temperature range 4-140K. Therefore this range was chosen for measurements of the new unknown samples.